Science of the Total Environment 926 (2024) 171837

Contents lists available at ScienceDirect

Science of the Total Environment

journal homepage: www.elsevier.com/locate/scitotenv

Responses of underground air and drip water geochemistry to meteorological factors: A multi-parameter approach in the Rull Cave (Spain)

M. Candela Ruiz [a,*], Concepción Pla [b], Angel Fernandez-Cortes [c], David Benavente [a]

[a] Department of Earth and Environmental Sciences, University of Alicante, C. San Vicente del Raspeig s/n, 03690 San Vicente del Raspeig, Alicante, Spain
[b] Department of Civil Engineering, University of Alicante, C. San Vicente del Raspeig s/n, 03690 San Vicente del Raspeig, Alicante, Spain
[c] Department of Biology and Geology, University of Almeria, C. Sacramento s/n, 04120 La Cañada de San Urbano, Almería, Spain

HIGHLIGHTS

- Radon in cave air responds to abundant rainfall.
- Radon activity is a tracer of water movement in the vadose zone.
- Prior calcite precipitation depends more on drip rate than cave air pCO_2.
- Rainfall $\delta^{18}O$ signature transfers to cave water only with prolonged rainfall.

GRAPHICAL ABSTRACT

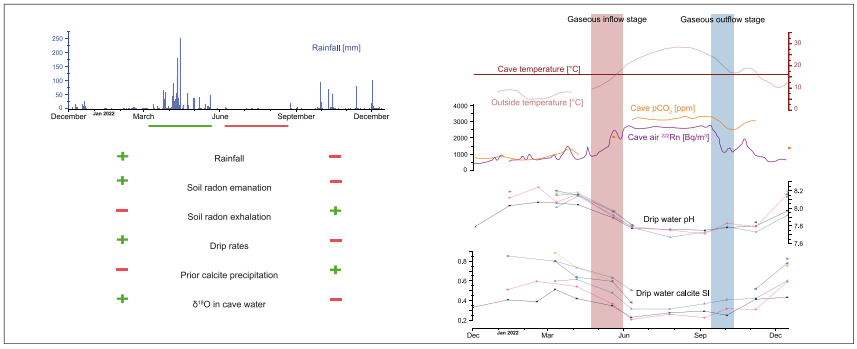

ARTICLE INFO

Editor: Christian Herrera

Keywords:
Microenvironment
Mediterranean climate
Karst
Radon

ABSTRACT

Our research aims to assess the complex interactions between the elements that constitute and influence a cave system through the analysis of an extensive dataset of climatic and environmental parameters (^{222}Rn, CO_2, drip rates, chemical composition, and environmental isotopes) measured in air, water, and solid in the Rull Cave (southeastern Spain). Of particular importance is understanding the effect of rainfall and temperature on water and gas transport through the epikarst and the involved processes. Our results show that the cave gaseous concentration patterns do not only depend on the temperature-caused movement of air masses, but they can also be affected by abundant rainfall. The $\delta^{18}O$ and δD composition of cave water also relies on such precipitations for the effective transfer of the rainfall signal into the cave, which can take between 3 and 7 days. The elemental ratios (Sr/Ca and Mg/Ca) show high responsiveness to the water drip rate, hinting that enhanced prior calcite precipitation (PCP) occurs at slower drip rates. Despite this, and regardless of drip rates, calcite saturation indices follow a seasonal variation pattern inversely proportional to the cave air CO_2 concentration, while $\delta^{13}C$-DIC is proportional. Our results show how the interlinkage between these multiple components defines the dynamics of the atmosphere-soil-cave system. Cave monitoring is then essential to understand the karstic vadose zone, which is highly sensitive to climatic influence and its changes.

* Corresponding author.
E-mail addresses: mcandela.ruiz@ua.es (M.C. Ruiz), c.pla@ua.es (C. Pla), acortes@ual.es (A. Fernandez-Cortes), david.benavente@ua.es (D. Benavente).

https://doi.org/10.1016/j.scitotenv.2024.171837
Received 20 December 2023; Received in revised form 29 February 2024; Accepted 18 March 2024
Available online 19 March 2024

1. Introduction

Caves are endokarst features developed within the vadose zone. They are the result of a complex interaction between multiple components: the overlying soil and the existing vegetation and microorganisms producing CO_2, the lithologies in which the cave is developed, the hydrosphere being the main variable as the dissolution/precipitation agent, and the atmosphere, the overall determining factor through climate. Caves are important elements for a wide range of academic disciplines, since they are repositories of geological, climatological, and even archaeological data, preserving information that would otherwise be lost due to surface erosion. In addition, often they are places for tourism and recreation, with health hazards that must be pondered beforehand such as potentially dangerous gaseous concentrations, primarily of CO_2 and radon (e.g., Dumitru et al., 2015; Alvarez-Gallego et al., 2015).

In particular, robust paleoclimatic reconstructions rely on detailed observation and monitoring of environmental parameters for understanding the signal transmission processes between regional climate, karst hydrology, cave microclimate and, finally, speleothem chemistry (e.g., Vieten et al., 2016; Voarintsoa et al., 2021; Zhang et al., 2023). A multidisciplinary understanding of the cave system is the essential first step for multiple research lines: the study of radon (^{222}Rn) in the system, a useful tracer gas (e.g. Csondor et al., 2017) but radioactive and a potential health hazard when accumulated in caves, the mobility of contaminant substances through soil and vadose zone, the assessment of groundwater quality and aquifer vulnerability, effects of wildfires, analysis of potential carbon sinks, and aquifer recharge assessment through infiltration quantification.

In a highly heterogeneous environment such as the karstic landscape, the characterization of these mechanisms and processes is not straightforward. Climate is a crucial factor, since it influences the amount and temporal distribution of water inflow, and it strongly conditions the vegetation cover, soil properties, and the carbonate system chemistry (Fairchild and McMillan, 2007). Cave water chemistry is predominantly a function of the groundwater residence time and its interaction with the overlying soil, cave host rock, and forming speleothems. Water pCO_2 usually increases on the path between soil and epikarst, and then might meet seasonally changing concentrations of CO_2, processes that altogether define speleogenesis and drip water geochemistry (Fernandez-Cortes et al., 2008).

Water discharge studies (e.g., McDonald and Drysdale, 2007; Fernandez-Cortes et al., 2008) display a wide range of hydrological responses to infiltration and their consequences on the system. Further studies also combine the analysis of geochemical changes using major dissolved ions (Fairchild et al., 2000; Huang et al., 2001; Musgrove and Banner, 2004), stable environmental isotopes of hydrogen, oxygen and carbon used to study infiltration, fractionation processes and water residence time in the vadose zone, and in paleoclimatic studies (Li et al., 2000; Kaufman et al., 2003).

This research reports on a comprehensive monitoring performed in Rull Cave, in Mediterranean southeastern Spain. The aim is to determine how the cave responds to meteorological parameters (rainfall and temperature), with particular emphasis in water geochemistry and dynamics. The Rull Cave, a relevant tourist enclave in the area, has been under monitoring for over a decade, and has therefore a well-defined background regarding microclimatic parameters and gaseous concentrations. Our study focuses, first, on CO_2 and radon (^{222}Rn) concentrations in soil and cave air to define the framework of gaseous dynamics during 2022. Second, and most importantly, we addressed the role of infiltrating water as vehicle for gas/solute transport, and the intermediate geochemical processes that occur in the upper vadose zone, particularly in terms of carbonate dissolution.

The study relies on a multi-parameter approach, integrating an extensive dataset of time series of cave and soil air composition regarding ^{222}Rn and CO_2, drip rate, water chemistry (main parameters, major and trace ions, isotopes of carbon, oxygen, and hydrogen), rainfall and temperature.

To achieve the main objective we (1) investigated seasonal variations in CO_2 concentration within soil and cave; (2) utilized the linkage between rainfall and radon activity in soil and cave air as tracer for air and water movements; (3) explored the combined impact of rainfall and cave air on drip water geochemistry and the implications for carbonate dissolution and precipitation; (4) analyzed water isotopes (δD, $\delta^{18}O$, $\delta^{13}C$) to unveil water-rock interaction processes and transmission of the isotopic signal, and (5) evaluated the hydrological connectivity between the surface and the Rull Cave by examining how rainfall conditions drip rates and transit time, which in turn influence water geochemistry.

The karst environment is characterized by intricate connections between geological, hydrological, geochemical, and even biological processes. Our study provides an integrated understanding of the complex interactions between atmosphere, lithosphere, and hydrosphere in the Rull Cave, considering potential environmental implications, effects on speleogenesis, cave ecosystems, and groundwater chemistry.

2. Studied cave

The Rull Cave (38° 48′ 40″ N, 0° 10′ 38″ W, 470 m.a.s.l.), Vall d' Ebo, Alicante, Southeast Spain (Fig. 1), is the result of the interaction between the outer atmosphere, soil, vadose zone, host rock, hydrosphere, and cave atmosphere subsystems. The cave environment shows intra-annual variations associated with seasonal changes and the related variations in temperature and rainfall distribution. These changes imply alterations in the physics–chemistry of the subsystems through the mobilization of solutes, and masses of water and air (Pla et al., 2023).

Above the cave, the soil is distributed in uneven patches and has a thickness below 1 m, with a fine to coarse texture and no differentiated horizons. Soil is composed of fine quartz (70 %), clay minerals (20 %), calcite (5 %) and feldspar (5 %) grains. The soil located above the Rull Cave is a silty-silty loam type, with a percentage of organic matter of 14.74 %. It has a bulk density of 1.13 g/cm^3, and a total porosity of 0.52 (Pla et al., 2017). Diverse C3 plants and Mediterranean vegetation grow in this soil profile (Pla et al., 2016a, 2017).

The Rull Cave is developed in massive, complex Miocene conglomerates which lay on Cretaceous limestones (altogether host rock). These

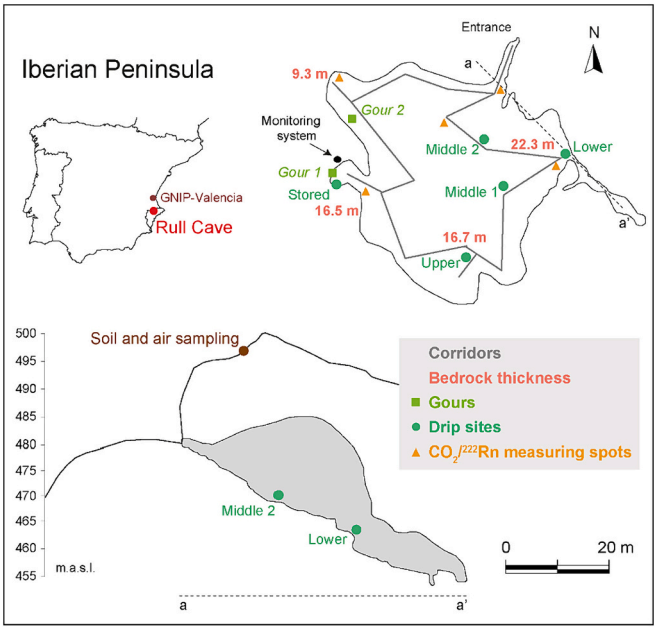

Fig. 1. Cave location and sampling sites. The colored labels next to the water sampling points (gours and drip sites) correspond to the given sample identifier. Modified from Nadal et al. (1990) and Pla et al. (2023).

conglomerates are composed of limestone clasts and calcite cement and matrix, the latter also having a minor amount of iron oxides, quartz grains, and clay minerals (Pla et al., 2016a, 2016b, 2017).

The cave is a roughly rounded single room with the entrance in the highest sector. It has an exposed surface of 1535 m^2 and contains 9915 m^3 of air. The height of the roof inside the main chamber is variable, with a maximum of 20 m (Fig. 1).

The cave contains several types of calcite speleothems such as stalactites, stalagmites, columns, flowstones, draperies, and fallen blocks product of past ceiling collapses (Pla et al., 2016a). There are also cave sediments laying across the floor, which consist of calcite, quartz, clay minerals, and feldspar. They originate from the transport of bedrock and soil components.

The Rull Cave area, located in a valley between mountains, has a Csa climate type, according to a slightly modified Köppen–Geiger Classification (AEMET-IM, 2011), with a mean annual air temperature of 16.1 °C and a dry, hot summer. The site has an average annual rainfall amount of 1041.68 mm, according to the 10 years series (2013−2023) recorded at the Vall d'Ebo climatic station (AVAMET, 2023). The largest amounts of precipitation are generally concentrated in spring and autumn, with a few exceptions (such as the winters of 2016–2017 with ~1040 mm, and 2019–2020 with ~700 mm).

During 2022, the AVAMET weather station in Vall d'Ebo registered 1971.8 mm, with 55 % occurred during March. Rainfall throughout the year was mostly concentrated in two periods, the first corresponding to meteorological spring (March to May), and the second to fall and the first month of winter (September to December). 26 days with rainfall >20 mm were recorded, and the maximum rainfall recorded in one day was 248.8 mm, on March 26, 2022 (Fig. 2).

During winter, the average mean air temperature was 8.96 °C, the average minimum was 3.03 °C, and the average maximum was 15.93 °C. During summer, the average mean temperature was 25.16 °C, the average minimum was 17.03 °C, and the average maximum was 32.33 °C (Fig. 2). The mean annual air temperature in 2022 was 16.7 °C.

The mean monthly evapotranspiration (calculated as proposed by Thornthwaite, 1948) is minimum from December to March (below 30 mm), and reaches maximum values between June and August, averaging 150 mm.

The cave atmosphere undergoes seasonal variations related to the contrast between the outdoor and the indoor air temperature, which is nearly constant and has an annual average of 16.2 °C (Pla et al., 2020). This difference determines the magnitude of the diffusive and advective fluxes, which are the controlling factors on the annual gas concentration cycles. When the air temperature outside is above the temperature inside the cave (summer), the higher air density inside the cave causes the inner atmosphere to remain isolated and stagnant, and the diffusive

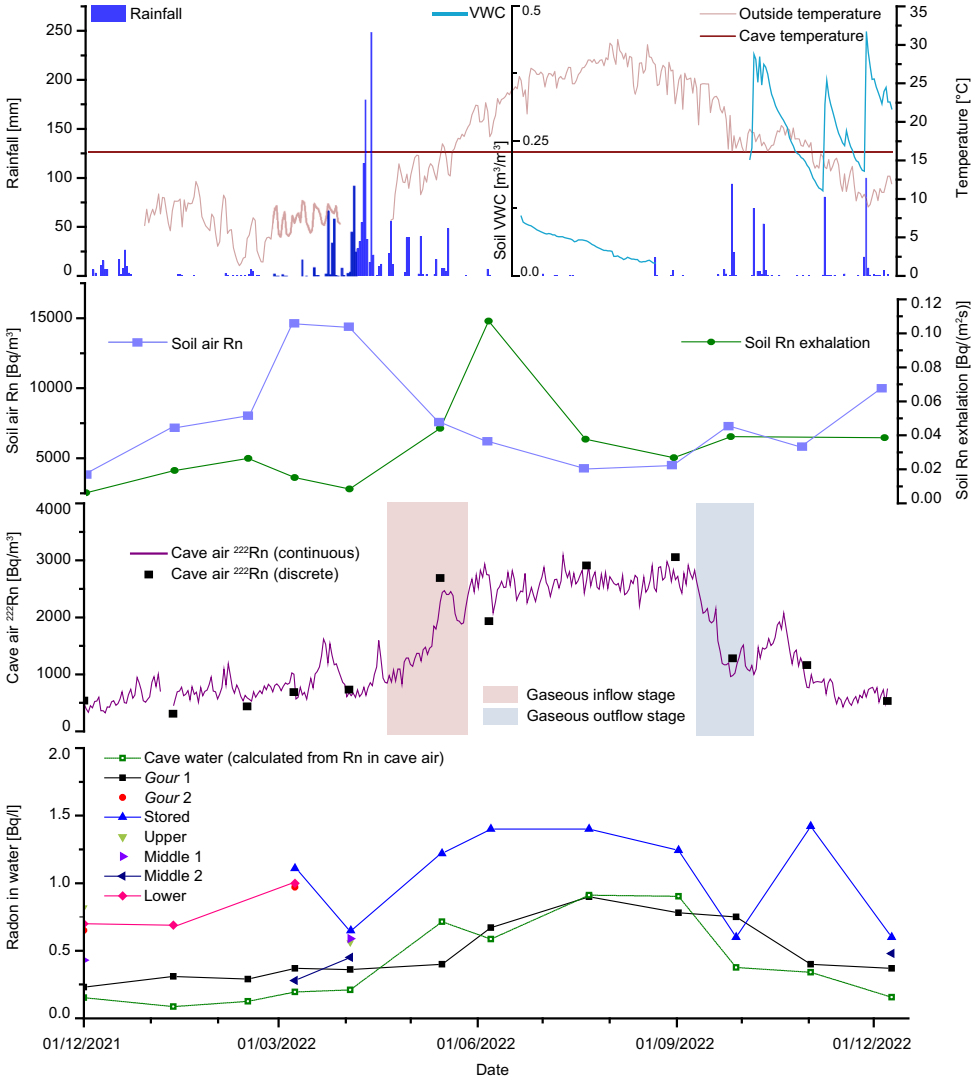

Fig. 2. (From top to bottom) Meteorological data, soil volumetric water content (VWC) and cave temperature. Soil radon activity in air and exhalation. Cave air radon measurements, with highlited gaseous inflow (accumulation) and outflow (ventilation) stages. Radon activity measured and calculated in water.

inflow of CO_2 and radon from the soil contributes to accumulate and increase the gaseous concentrations in cave air. When the temperature gradient is inverted, the cave is not isolated from the exterior atmosphere and the advective outflow lowers the gaseous concentrations. This results in four distinct consecutive stages: gaseous diffusive inflow into the cave, (coincident with the spring-summer transition), maximum gas concentration in the cave (summer), gaseous outflow (summer–autumn), and a period in which the gas concentration reaches minimum values (winter) (Pla et al., 2020).

The average relative humidity of the cave air is close to saturation (97.8 %, Pla et al., 2020), with reduced seasonal variation. The water inside the cave can be found in the form of pond-like accumulations —called *gours*—, or active drip sites. These *gours* are formed in specific locations in the cave that allow the accumulation of small volumes of water, with a maximum of 2–3 m^2 of water surface and up to 40 cm deep. The volume of water varies seasonally, in response to the amount of water entering the cave through dripping sites, distributed throughout the cave.

3. Methodology

Specific parameters were monitored by installing different sensors in the ground and in the cave, allowing us to obtain continuous data series. In parallel, sampling visits were conducted over 13 months between December 2021 and December 2022, with an approximately monthly frequency except for the period July–August, which had a single sampling visit at the end of July.

3.1. Local weather conditions

The meteorological data for the studied area was obtained from the Vall d'Ebo climatic station, located 1.7 km from the Rull Cave. The weather station belongs to the network of the "Valencian Association of Meteorology *Josep Peinado*" (AVAMET, 2023). The station provides daily data on precipitation, relative humidity, atmospheric pressure, wind intensity, and temperatures.

Monthly atmospheric air samples were taken above the cave in 1 l bags for the measurement of the atmospheric isotopic signal of carbon ($\delta^{13}C$) in gases (CO_2 and CH_4) at the facilities of the Stable Isotope Laboratory (University of Almería) using a Picarro G2201-i Analyzer.

The rainfall δD and $\delta^{18}O$ compositions were obtained from the measurements in the city of Valencia, located approximately 70 km from the cave (Fig. 1). The data (reported relative to Vienna Standard Mean Ocean Water—VSMOW—) were provided by the Spanish Network for Isotope Monitoring in Precipitation (REVIP, 2023) which belongs to the Global Network for Isotopes in Precipitation (GNIP), managed by the Center for Studies and Experimentation of Public Works in collaboration with the State Meteorological Agency.

3.2. Soil air and solid analyses

All soil related analysis and sampling were conducted at the same location above the cave, as shown in Fig. 1.

CaO and MgO concentrations were obtained for a soil solid sample using ME-ICP06 (Fusion decomposition followed by ICP-AES measurement), and Sr concentration using ME-MS41 (Lithium borate fusion followed by acid dissolution and ICP-AES measurement).

The isotopic composition of carbon ($\delta^{13}C$-bulk and $\delta^{13}C$ of organic carbon) in the soil solid fraction was analyzed using the Picarro G2201-i Analyzer coupled with a Combustion Module designed by Costech Analytical (NC Technologies) at the University of Almería. All $\delta^{13}C$ data in this study are reported relative to Vienna Pee Dee Belemnite (VPDB).

Discrete soil air samples were taken monthly for CO_2 and radon measurement. Air was extracted with a battery pump from three steel tubes inserted 0.4 m into the ground. The air stored in 2 l Tedlar sampling bags was analyzed to measure radon activity using AlphaGUARD DF2000 (Saphymo GmbH, Frankfurt am Main, Germany) set in 1-min flow mode, with a 0.3 l/min pump flow, over a 15-min period. AlphaGUARD uses the principle of pulsed ionization chamber (alpha spectroscopy), in which radon activity is measured in Bq/m^3. The air stored in 1 l Ritter sampling bags was analyzed to characterize the temporal variation of the soil air CO_2 concentration and its $\delta^{13}C$ signature using the Picarro G2101-i analyzer.

Radon exhalation from the soil, E ($Bq/(m^2s)$), was estimated in an accumulation chamber of PMMA (polymethyl methacrylate), with a diameter of 20 cm inside. The chamber was located over a single PVC collar permanently installed in the soil. The accumulation initially describes a linear growth with time, t (s), of the radon activity in the accumulation chamber, CRn (Bq/m^3). Radon exhalation (E) is calculated as follows (Eq. (1)):

$$E = \frac{V}{S} \times \frac{C\mathrm{Rn}}{t} \quad (1)$$

where V (m^3) is the effective volume of the accumulation chamber and S (m^2) is the surface of soil within the chamber. Radon activity was recorded using an AlphaE (Saphymo GmbH, Frankfurt am Main, Germany) for 4 h each time.

A HOBO U12 logger (Onset, USA; accuracy of ±0.5 °C) and an ECHO EC-5 probe (Decagon Devices, USA; accuracy of ±1–2 %) connected to an Em5b logger (Decagon Devices, USA) were installed to hourly measure the soil temperature and volumetric water content (VWC). The probes are located 10 cm into the ground.

3.3. Cave air, solids, and drip water analyses

The solid components found inside the cave (host rock, speleothems, and cave sediments) were sampled and analyzed to obtain the isotopic composition of carbon following the same methodology detailed for soil (Section 3.2). The speleothems were sampled near *Gour* 1 and Stored sites (Fig. 1), collecting the uppermost layer of the flowstone in which *Gour* 1 accumulates. All solid samples were analyzed to obtain CaO, MgO (via ME-ICP06), and Sr (via ME-MS41) concentrations.

Microclimatic measurements were taken within the cave using a HOBO H22-001 datalogger manufactured by Onset Computer (USA). The monitoring system is in a secluded area of the cave that is off-limits to visitors (Fig. 1). The datalogger is connected to various probes, which provide hourly readings of temperature and relative humidity (HMP45AC, Vaisala, Finland, with an accuracy of ±0.2 °C and ±2.0 % respectively), CO_2 concentration (GMP252, Vaisala, Finland, with an accuracy of ±40 ppm and a measurement range of 0 ppm to 10,000 ppm), and barometric pressure (S-BPB-CM50 Sensor, Onset Computer, USA, with an accuracy of ±3.0 mbar). Furthermore, an hourly monitoring of radon activity in the air was performed using a Radim 5WP radon monitor (SSM&SISIE, Prague, with an accuracy of ±12 Bq/m^3).

Approximately every month, discrete air samples were taken from the cave in five homogeneously distributed sites (Fig. 1). Air was pumped into 1 l Ritter and 2 l Tedlar sampling bags. The sampled air was used to measure radon activity, CO_2, and $\delta^{13}C$-CO_2, following the methodology used for soil air analysis, detailed in the previous section (Section 3.2). All measuring points had similar gas concentrations and followed similar patterns throughout the studied period. The average of the standard deviations calculated for each monthly set of five measurements is 60 ppm for CO_2, and 90 Bq/m^3 for radon. Since these deviations are not relevant for the scope of this study, which focuses on the evolution in time, we selected a single sampling point (located next to the Lower drip site, shown in Fig. 1) as representative of the CO_2 concentration and radon activity in cave air.

The two largest water accumulations inside the cave were selected for monitoring: the first and largest, named *Gour* 1, has a variable volume of water throughout the year, without drying out during the period studied. The second most important pond, called *Gour* 2, is conditional

upon the occurrence of heavy rainfall events. Four dripping sites were selected within the main cavern (Fig. 1) based on the following criteria: representation of different sectors inside the cave, diverse dripping rates and seasonal behaviors, and feasibility of installing sampling containers. Due to the vaulted architecture of the cave and the fact that the drips fall from a height between 15 m and 20 m, the water was collected in open 500 ml containers. A fifth drip site was monitored in the upper part of the cave, above *Gour* 1 (Fig. 1): a 10-liter PET plastic recipient with a neck of 3 cm was placed, with a funnel located above and connected through a tube, set to collect on every visit the water accumulated from the dripping of up to 10 stalactites. These stalactites had an irregular and slow drip rate. In all visits, the bottle, tube, and funnel were found full of water.

At these selected sites, subject to the available water volume, in situ water parameters (temperature, electrical conductivity, total dissolved solids, pH) were measured using a HANNA HI98194 portable meter equipped with a multiparameter pH/EC/DO/Temperature probe (HI7698194). The water was sampled in polypropylene recipients for different purposes: 5 ml tubes for trace elements analysis using ICP-MS, 50 ml for analysis of major ions using ion chromatography (DIONEX DX 500), 50 ml for determination of bicarbonates through neutralization titration (methyl orange and 0.01 N HCl), and 50 ml for the isotopic analysis. δ^{13}C-DIC of water was measured using a Picarro G2201i coupled through Picarro A0301–Liaison with a Picarro A0302–Automate FX, for CO_2 generation for water-dissolved inorganic carbon (DIC). δD, δ^{18}O and δ^{17}O of water were measured with Picarro L2140i Analyzer coupled with Picarro Autosampler A0325 and a highly stable vaporization system (Picarro A0211). All samples were stored in a refrigerator (approximately 4 °C) until analysis. In addition, 100 ml or 500 ml of water were sampled, depending on availability, in airtight amber glass containers to measure radon activity using AlphaGUARD DF2000 coupled with AquaKIT (Saphymo GmbH).

CO_2 partial pressure and mineral saturation indices (SI) in water were calculated using *Phreeqc* Interactive version 3.7.3 (Parkhurst and Appelo, 2013). The theoretical partial pressures of CO_2, in equilibrium with every water sample, were obtained from the CO_2 saturation calculated by *Phreeqc*, expressed in atm, and subsequently converted to ppm.

The activity of radon in water (CRn_{water}, Bq/l) calculated in equilibrium with the activity measured in air (CRn_{air}, Bq/m^3) (i.e., the theoretical activity of radon in water, namely "cave water"), was obtained by means of the equation (modified from Schubert et al., 2006, Eq. (2)):

$$CRn_{water} = \frac{CRn_{air}}{1000} \times \left(0.105 + 0.405 \times e^{-0.0502T}\right) \quad (2)$$

With T being the temperature (°C).

The radon activity after a certain amount of time (i.e., after decay) was calculated using the solution of the equation for the time evolution of the parent isotope (the same as for a single step decay), originally obtained from the Bateman equation (a mathematical model describing abundances and activities in a decay chain as a function of time, based on the decay rates and initial abundances, Eq. (3)).

$$CRn(t) = C_0 e^{-\lambda t} \quad (3)$$

With CRn being the calculated radon activity (Bq), $\lambda = 0.00761$ (h^{-1}, Alonso-Hernández, 2016), t being time (h), and C_0 being the radon activity (Bq) at $t = 0$.

4. Results

4.1. Soil properties, air, and solid composition

The soil above the Rull Cave is a silty-silty loam, medium-textured soil composed of quartz, clay minerals, calcite, and feldspar. The contents of CaO and MgO in soil, relevant for this study, are 2.22 % and 1.18 %, respectively. The Sr concentration is 79.7 ppm.

Soil temperature responds to variations in atmospheric conditions. The average soil temperature in winter is 7 °C, and in summer 26.25 °C. The soil volumetric water content (VWC) is closely related to the volume and intensity of rainfall, and the temperature of the atmosphere and soil. Due to an electric failure in the measurement equipment, VWC data for the year 2022 is limited to a few months. However, it is sufficient to see the strong and immediate response of soil moisture to rainfall (Fig. 2). On a daily scale, the VWC of the soil increases associated with precipitation, even reaching values remarkably close to the soil porosity, and decreases in the following days depending on the temperature. The soil VWC is higher in the rainy seasons (spring and autumn) and in winter, when the rainfall is less significant, but the lower temperatures allow the soil to retain moisture for longer. During summer, the scarce rainfalls and high temperatures cause the VWC to reach minimums below 0.1.

The gases studied in soil air are CO_2 and ^{222}Rn. The measured radon activity peaks were measured in March and April, with above 14,000 Bq/m^3 (Fig. 2). The minimum activities of radon, around 4000 Bq/m^3, were measured in December 2021 and summer 2022. The exhalation of radon from the soil into the atmosphere has varying values throughout the monitored period. In general, radon exhalation is lower during and immediately after rainfall.

The highest soil CO_2 concentration (close to 5000 ppm) was recorded in May, while the lowest concentrations (close to 1500 ppm) were measured in winter, when temperatures are minimal, and in summer, when soil moisture is minimal (Fig. 3).

The stable carbon isotope composition (δ^{13}C-bulk) measured in the soil is −26.28 ‰ ± 0.07 ‰ (Fig. 4). The isotopic composition of carbon in CO_2 in soil air varies throughout the year. Between June and September, when temperatures are higher, the average δ^{13}C-CO_2 value is −19.83 ‰. During the rest of the year, the value of δ^{13}C-CO_2 oscillates between −20.3 ‰ and −24.9 ‰ (Fig. 4), with a mean of −23.03 ‰, as expected for the existing C3 vegetation.

4.2. Solid, air, and drip water characterization in the cave

4.2.1. Characterization of the solid fractions

As previously stated, the cave has three different lithologies: the breccias and conglomerates in which the cave has developed (host rock), the speleothems precipitating inside the cave, and the cave sediments distributed throughout the cave floor.

Regarding the chemical composition relevant for this study, the host rock has 58 % CaO, 0.18 % MgO, and 79.7 ppm of Sr. The uppermost layer of the flowstone below *Gour* 1, referred as speleothem, has 57.3 % CaO, 0.03 % MgO, and 10.1 ppm of Sr. The cave sediments have 23.8 % CaO and 0.84 % MgO. They have important amounts of trace elements, with a composition similar to that of the soil overlying the cave. The Sr concentration is 82.2 ppm. The isotopic composition of carbon in the host rock (δ^{13}C-bulk) is −1.78 ‰ ± 0.07 ‰ (Fig. 4). The measured speleothem has a δ^{13}C-bulk of −9.47 ‰ ± 0.03 ‰ and the cave sediments δ^{13}C-bulk is −11.25 ‰ ± 0.44 ‰, with δ^{13}C-organic −16.45 ‰ ±0.16 ‰ (Fig. 4).

4.2.2. Cave atmosphere: parameters and gaseous composition

The average pressure inside the cave is 966 mPa, with no seasonal trends observed. Temperature varies only slightly throughout the year (annual average of 16.2 °C): the minimum values are around 15.2 °C in June, and the maximum values of around 16.3 °C in December (according to data measured in 2021).

The radon activity measured in cave air follows a seasonal pattern: from December to May it has a base activity between 500 Bq/m^3 and 1000 Bq/m^3, with isolated activity peaks, and from June to September it has 2500 Bq/m^3 to 3000 Bq/m^3 (Fig. 2), similar to the averaged values of previous years (Pla et al., 2023).

The CO_2 concentration varies between 500 ppm and 1000 ppm (from December to April, when the cave is ventilated), and rises progressively

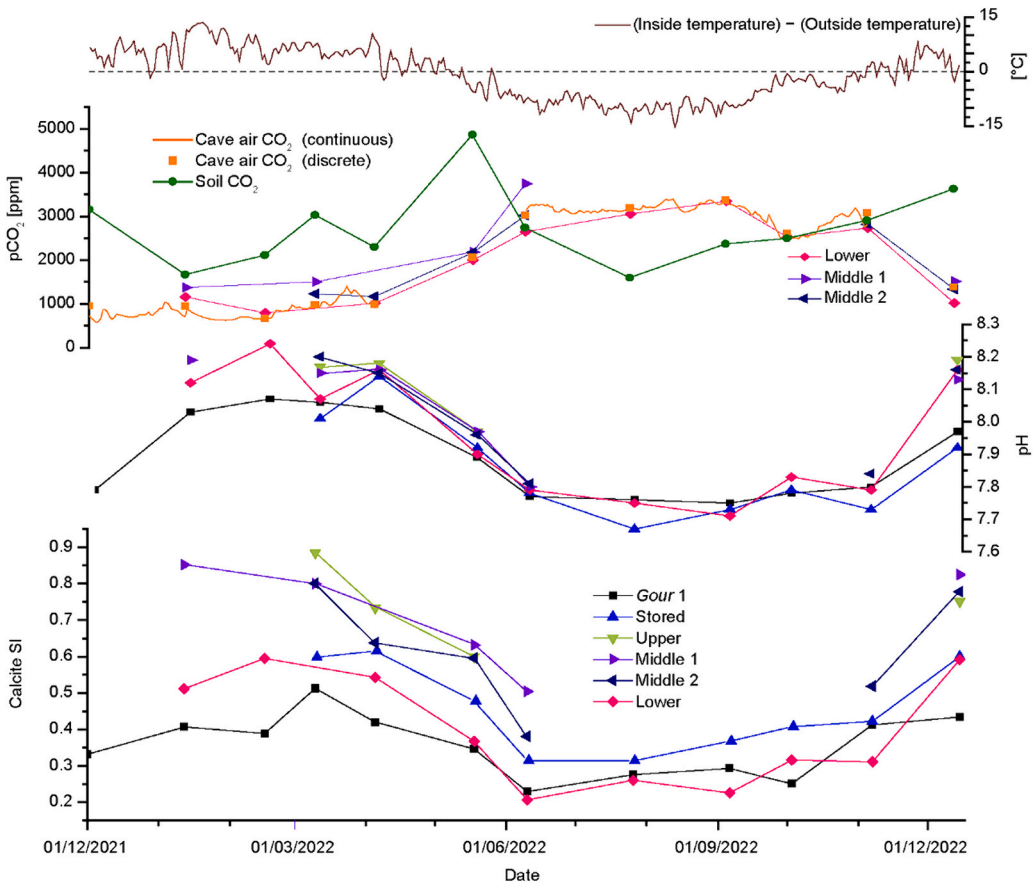

Fig. 3. (From top to bottom) Temperature difference between the cave (inside temperature) and the atmosphere (outside temperature). CO_2 concentration in soil and in cave air. pH of water samples in the Rull Cave. Calcite saturation indices in water.

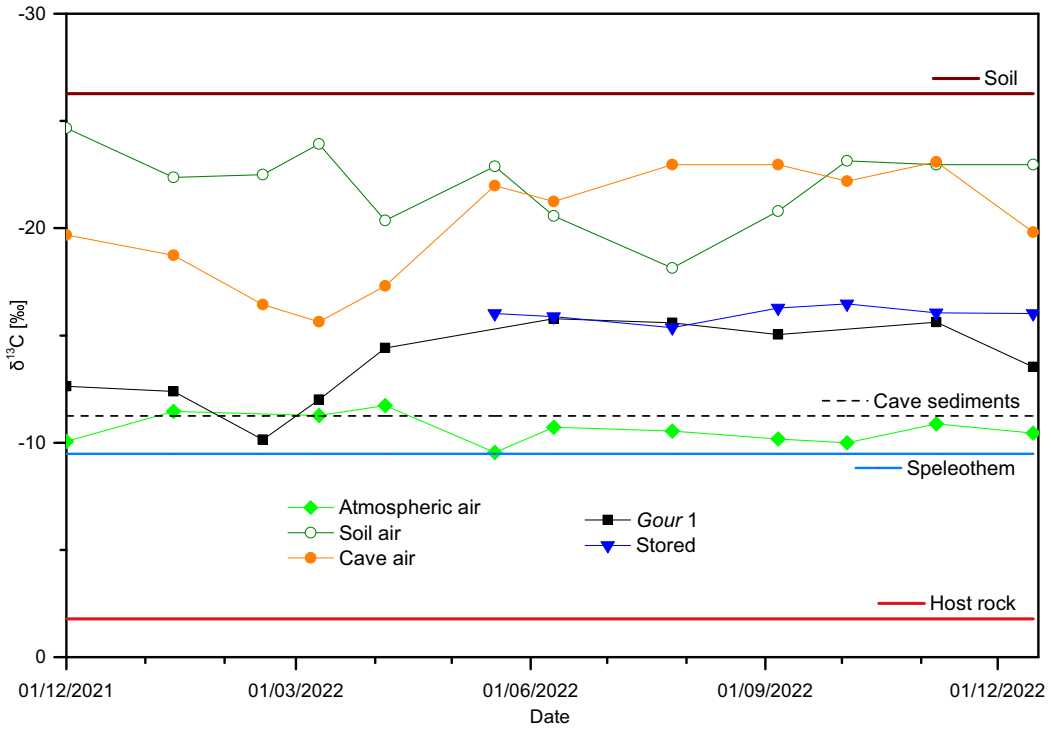

Fig. 4. δ^{13}C-bulk composition for all solid phases in the Rull Cave. δ^{13}C-CO_2 measured in the atmosphere, cave air and soil air. δ^{13}C-DIC measured in the water inside the cave, at Gour 1 and Stored sites.

to values from 2500 ppm to 3000 ppm (between June and November, when the cave is isolated) (Fig. 3). These values are slightly below those recorded in previous years (Pla et al., 2023). The carbon isotopic composition of CO_2 ($\delta^{13}C\text{-}CO_2$) in cave air pattern shows a seasonal variation coincident with changes in cave air CO_2, with a heavier isotopic composition when the cave was ventilated, and a lighter composition when the cave air stagnates (Fig. 4). The highest $\delta^{13}C\text{-}CO_2$ was measured during March 2022.

The carbon isotope composition of CO_2 ($\delta^{13}C\text{-}CO_2$) in cave air shows a variation that results of the mixture of CO_2 from the background atmosphere and soil-derived CO_2 (isotopically light CO_2-rich air) that reaches the cave environment by diffusion, advective air fluxes and by degassing from seepage water. During the colder months, when the cave is ventilated and influenced by atmospheric air which has a $\delta^{13}C\text{-}CO_2$ value roughly constant at around −10 ‰, the air in the cave shows a higher $\delta^{13}C\text{-}CO_2$ (Fig. 4). When the cave air is stagnant during the summer, the $\delta^{13}C\text{-}CO_2$ values are lower and more similar to those obtained in the soil air (Fig. 4).

4.2.3. Drip water properties and composition

The volume of water in the *gours* and the dripping rates depend on the precipitations. The Stored drip site, collected monthly, produced a minimum of 10 l every 3–4 weeks throughout the studied period. The Lower drip was found to be the only drip site active in all visits (Fig. 5).

All water samples are calcium bicarbonate type, in accordance with the geological context. In general, electrical conductivity (EC) does not show a strong seasonal trend, except for a general slight increase between April and June, a pattern observed also for HCO_3^- and Ca^{2+} (Figs. S1 and S2 in Supplementary material, respectively). There are consistent differences between sampling sites, with almost all drip sites having higher EC (between 300 μS/cm and 400 μS/cm) than *Gour* 1 and Lower (both between 200 μS/cm and 300 μS/cm) (Fig. S3). Other major ions show generally stable concentrations throughout the year (Tables S1 to S6), without seasonal trends or relevant differences between the sampled sites. Among trace elements, Sr has a different behavior, with *Gour* 1 and Stored having larger amounts than the other drip sites (Fig. S4). There are no identifiable trends at any sampling site.

There is a decrease in pH in all samples during summer, following a strong seasonal trend (Fig. 3). Calcite, the main dissolved carbonate mineral species analyzed, is shown to be always slightly supersaturated, with saturation indices (SI) between 0 and 1. The saturation indices also follow a seasonal pattern (Fig. 3), being comparatively lower between June and October. The water collected from the Upper and Middle 1 and 2 drips has a calcite SI higher than those of the remaining sites. The samples of *Gour* 1 and Lower drip site show similar SI.

The measurements of radon activity in water inside the cave show values below 2 Bq/l (Fig. 2). The most complete series, obtained from *Gour* 1, shows an intra-annual activity variation approximately coincidental with the pattern of radon in the cave air. This is further corroborated with the theoretical water radon, calculated using the activity in air, which shows the same pattern and amounts of radon as *Gour* 1 (Fig. 2). In summer, radon activity in *Gour* 1 averages 0.77 Bq/l, while the rest of the year averages 0.3 Bq/l. The monitored drip sites and *Gour* 2 show higher radon activities of up to 0.8 Bq/l, even during winter when cave air radon is at its lowest. The Stored drip shows values significantly higher than all other sites in most measurements, reaching up to 1.4 Bq/l (Fig. 2).

$\delta^{13}C$-DIC was measured in *Gour* 1 water in all visits except two, and in Stored drip between May and December 2022 (Fig. 4). All samples show values between −16.5 ‰ and −10 ‰ (Fig. 4).

Regarding $\delta^{18}O$ and δD, the data pairs of isotopic composition of the water collected in Rull Cave have a defined trend line (Fig. 6). The monthly averages of the $\delta^{18}O$ and δD data obtained from the GNIP station in Valencia (Fig. 1) show strong seasonal tendencies, with the three summer months having the heaviest rainfall isotopic composition, and the three winter months the lightest (Fig. 6). In accordance with these annual trends, the measurements in *Gour* 1 show a lighter isotopic composition from December to March.

5. Discussion

5.1. Influence of meteorological parameters on radon in the Rull Cave

Radon activity in soil air is the result of, first, the generation of ^{222}Rn through radioactive decay of radium (^{226}Ra) — and ultimately from ^{238}U—, and afterwards radon emanation, when a fraction of the produced isotope enters the poral space. Radon generation depends on the uranium concentration in soil (3.14 ppm above the Rull Cave, according to Pla et al., 2023). Radon emanation relies on soil parameters such as water content, texture, and ambient temperature (Nazaroff, 1992; Phong Thu et al., 2020). Therefore, radon in soil air is closely related to weather. As seen in Fig. 2, soil radon activity increases during rainy periods and when the VWC of soil is higher, promoting radon emanation (Sakoda et al., 2010). Although the March and April measurements have a large difference in the volume of precipitation within the previous days, the radon values are similar, thus possibly approaching the maximum soil radon activity above the Rull Cave. The minimum values were measured in summer, when the soil moisture content is at its lowest (Fig. 2).

Radon exhalation (flux from the soil to the outside atmosphere) is influenced by the soil radium content, soil water content and surface soil temperature (Hosoda et al., 2007; Modibo et al., 2021). Soil water content of up to an estimated 8 % can have positive effects on radon exhalation (Hosoda et al., 2007). Above 8 %, there is a predominant reduction in radon diffusion (Cothern and Smith, 1987) since liquid water causes a decrease in soil porosity and permeability (Nazaroff,

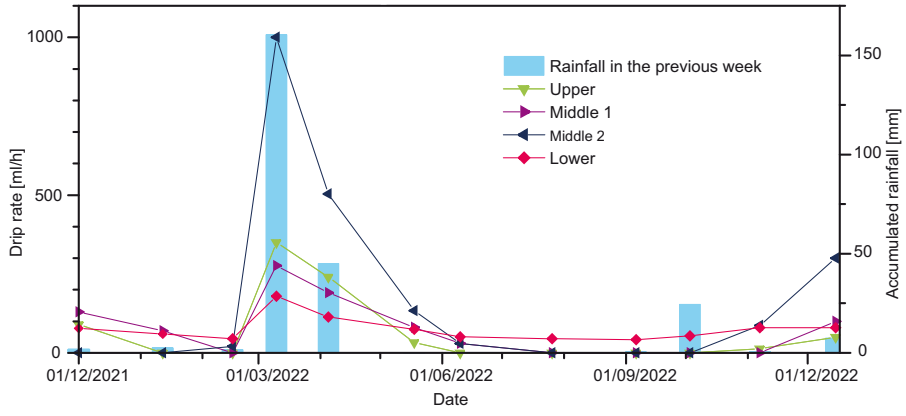

Fig. 5. Drip rates measured in the Rull Cave compared with the rainfall accumulated in the seven days prior to the drip rate measuring.

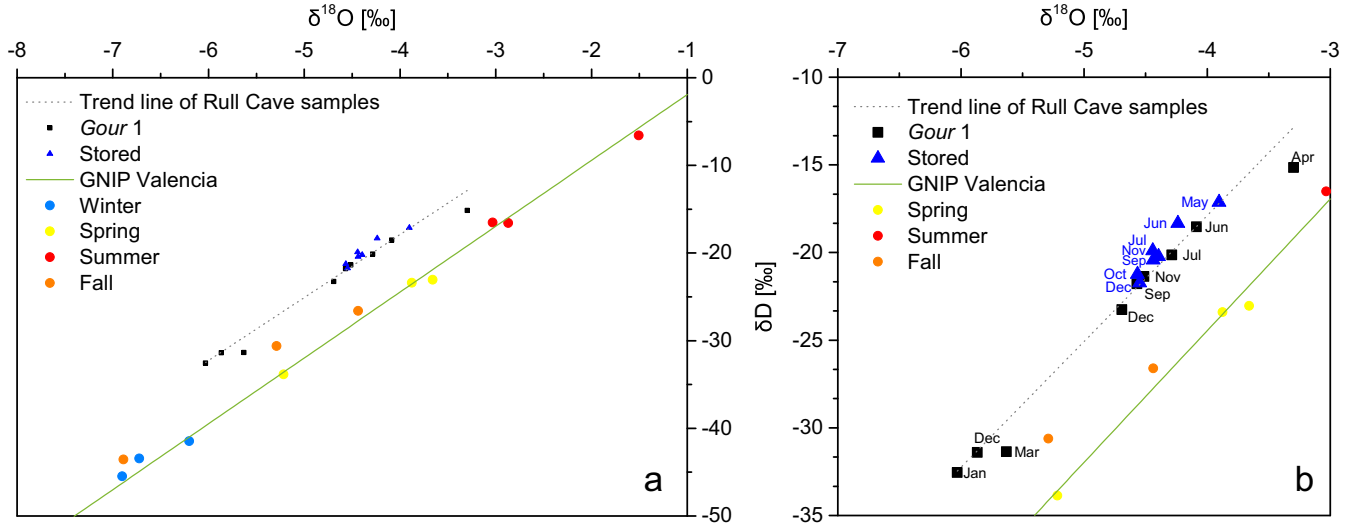

Fig. 6. (a) $\delta^{18}O$ and δD composition for rainfall (solid line, data from Valencia GNIP station, $\delta^{2}H = 7.512 \times \delta^{18}O + 5.589$) and sampled water in Rull Cave (dotted trend line). The monthly $\delta^{18}O$ and δD averages of the Valencia station (circles) are colored according to meteorological season. (b) Zoom in to the Rull Cave water samples, labeled with the month of sampling.

1992; Maeng et al., 2019). Consistent with previous studies (e.g., Gavriliev et al., 2023), radon exhalation is higher during summer and reaches its minimum in March and April, when the most abundant rainfall is recorded (Fig. 2). Thus, radon activity in soil air and soil exhalation show, in general, opposite behaviors.

Inside the Rull Cave, radon activity in air mostly depends on the ventilation processes triggered by the difference between outside and inside temperature (Pla et al., 2023). As previously stated, the Rull Cave has four distinct stages. The gaseous inflow (accumulation) and outflow stages are defined by the existence of 10 consecutive days with an absolute variation of 500 Bq/m^3 in radon activity. The radon accumulating inside the cave has its source in the sediments found in the cave, and in the soil (2.23 ppm and 3.14 ppm of uranium, respectively, Pla et al., 2023). The maximum and minimum gas concentration stages are determined by the occurrence of 10 consecutive days without variations in gas concentrations. The cave gaseous inflow and outflow stages are clearly visible during the studied period (Fig. 2). There is an increase in radon (and CO_2) in October, near the end of the air outflow stage, most likely related to a combination of three factors: abundant rainfalls in early October (e.g., as listed in Table 1) triggering radon emanation and CO_2 production in the soil, constant radon emanation from the cave sediments, and a visible increase in the outside temperature (Fig. 2). This temperature gradient causes, as in summer but to a lesser extent, the colder cave air to stagnate.

Considering this, the data measured in 2022 show that, under certain circumstances, the cave atmosphere may experience significant changes outside these delimited stages. In the Rull Cave it was observed that, as previously described in Pla et al. (2020), daily rainfall <77 mm does not cause changes in radon activity in the cave air. On the contrary, daily rainfall >77 mm can trigger increases in radon activity (Pla et al., 2020). As shown in Table 1, in 2022 for a meteorological event to produce changes in the composition of cave air, two conditions must have been met: a minimum daily rainfall >70 mm, and significant precipitation must occur in the following days. The peak radon activity in the cave atmosphere is reached in 4 to 6 days after the first rainfall, similar to what was observed in Pla et al. (2020).

This is possible due to rainfall triggering several subsequent processes: an increase in radon emanation in the soil (Sakoda et al., 2010), a piston-like effect displacing the gas from the soil into the cave, and the transport of radon dissolved in water. Sustained precipitation on the days following heavy rainfall maintains soil VWC high. With a higher percentage of pores occupied by water, radon exhalation to the outside atmosphere is hindered (Benavente et al., 2019). This is corroborated by the decrease in radon exhalation measured during or immediately after precipitation. With the infiltrating water acting as a physical barrier, a piston-like effect (Pu et al., 2014) takes place and the radon produced and stored within the soil and vadose zone is displaced into the cave. The fact that reaching the peak radon activity in cave air takes between 3 and 7 days is a potential indicator of the time it takes for the infiltrating rainfall to reach the cave. Since radon solubility in water decreases with temperature, the precipitations produced from fall to spring are likely to provide appropriate conditions for higher solubility, and dissolved radon may then migrate over longer distances (Kulali et al., 2017).

During summer, when the cave air is stagnant, the combination of high radon values in the cave and scarce rainfalls (Fig. 2) impedes the occurrence of this effect. During the gaseous accumulation and outflow stages of the cave, there are no effects that could be specifically attributed to rainfall due to a higher volatility of the cave atmosphere.

Furthermore, the extraordinary rainfall that occurred on March 16

Table 1
Meteorological events with the most abundant rainfalls in the studied period, and the radon activity response in the air inside the cave.

Starting date	Total rainfall [mm]	Rainfall duration [days]	Total rainfall in the following 6 days [mm]	^{222}Rn increment [Bq/m^3]	Days to reach peak ^{222}Rn activity
04/03/2022	157.8	4	8.6	300	5
16/03/2022	893.4	12	22.2	1034	7
04/04/2022	90.4	3	3.2	0	–
12/04/2022	81.4	3	42.6	895	6
20/04/2022	40	1	2.8	0	–
06/10/2022	70	1	64	492	4
11/10/2022	59	2	0.6	0	–
11/11/2022	80	1	1.8	0	–
01/12/2022	127.6	3	3	170	5

(Table 1) also produced an increase in the CO_2 concentration in cave air of around 450 ppm relative to the concentration before the rainfall (visible in Fig. 3). This CO_2 increase in March was also measurable in soil air (Fig. 3).

Since drip water falls from over 10 m high at all sampling sites, the degassing effect cannot be negligible. Even in these circumstances of radon loss, the activity in drip water is equal or higher than the measured in *Gour* 1 and the calculated theoretical activity in "cave water" (Fig. 2). This is a potential indicator that the original amounts of dissolved radon were significantly higher, and that the radon source in drip water is not the cave air but the overlying solid phases of the system, i.e., soil and host rock.

The low sampling density for radon measurements in water does not allow for a statistical correlation between soil radon and drip water radon. However, the radon measured in the Stored drip in March (before the gaseous diffusive inflow stage) is comparable to the measurements in the stagnant cave air stage. Although *Gour* 1 is in dynamic equilibrium with the radon in cave air, the sampled water does not show variations linked to rainfalls. The increases in cave air radon associated to rainfall do not produce measurable changes in *Gour* 1, but they might be measured in drip water sites such as Stored, since they respond to soil radon activity (Fig. 2).

To summarize, the soil-produced radon likely has a minimum time to reach the cave of 3 days. This is further corroborated by applying the inverse of the decay equation (Eq. (3)) to the measured air radon activity with 3 days of decay reversed. When the cave air is stagnant (summer), the "original" radon activity before 3 days of radioactive decay is equal to the activity measured in soil air for the same period (Fig. 7). Radon activity in cave air depends then on three main factors: the emanation capacity of the most radioactive sources in the system (soil, cave sediments, and host rock), radon exhalation and transport time through the vadose zone, and radon decay rate. In summer, without the inflow of radon-poor air from outside, the cave air radon tends toward dynamic equilibrium with soil radon, one of the highest radon-producing components of the system.

5.2. Drip rates response to rainfall

The drip rates and response time to precipitations are determined by the amount of water entering the system, and the configuration of the vadose zone. It is possible to outline the relationship between drip sites activity and rainfall as proposed, for example, by Baker et al. (2020) and Baker et al. (2021). To corroborate the previously estimated response time, the drip rates (Fig. 5) were compared with the absolute and accumulated rainfall volumes. Fig. 8 shows the coefficients of determination (R^2) between the drip rates and the rainfall amount recorded on each day prior to measurement of the drip rate (Fig. 8.a), and the R^2 between the drip rates and the accumulated rainfall amount recorded n days prior to drip rate measuring (Fig. 8.b). Fig. 8.a shows that the drip sites have a higher response to the rainfall occurring 3, 4 or 6 days before and, to a lesser extent, 7 days before. Likewise, Fig. 8.b shows that all drip sites have a response time to rainfall between 3 and 7 days.

The estimated response time of 3 to 6–7 days corresponds to the transit time of water in the vadose zone after rainfall, until reaching the cave. The time interval matches with the time frame estimated for the radon transport from soil to cave, supporting the role of infiltrating water as both means of transport and physical barrier for soil gases (Pu et al., 2014).

The response time of the drip sites to rainfall is not always equivalent to the water residence time in the vadose zone above the Rull Cave. There are drip sites (such as Lower, Fig. 5) active even during prolonged periods without rainfall (such as Lower, Fig. 5) like summer 2022, with approximately 100 days totaling only 30 mm (visible in Fig. 2). It is fair to assume that there is an overlying water reservoir above this point continuously supplying water. For this reason, it is likely that the water residence time in the epikarst is significantly longer than the estimated response time to heavy rainfall. The thicker vadose zone overlying Lower drip site, when compared to other drip sites (Fig. 1), is expected to be a relevant factor influencing the residence time.

5.3. Hydrochemistry

The main factors controlling drip water chemistry are climate and weather, water residence time in the vadose zone, soil and host rock lithology, and the dynamics of cave gases (Tooth and Fairchild, 2003; Zhou et al., 2011). The relative importance of each factor varies at different temporal and spatial scales. CO_2–water interaction is one of the most important processes in carbonate environments, controlling both carbonate dissolution and deposition (Dreybrodt, 1999). Meteorological conditions are also of influence through its related parameters, such as soil VWC, soil and air temperature (and the associated gradients), wind speed, and air pressure (see, e.g., Schubert and Schulz, 2002).

CO_2 inside the Rull Cave has its origin in the soil above (Pla et al., 2023). Soil CO_2 is the combination of CO_2 produced by microbial activity, root respiration, and decomposition of organic matter (Breecker et al., 2012), and its production increases along with temperature and soil moisture (Fang and Moncrieff, 2001) but without reaching water saturation, since it prevents microbial activity and limits soil respiration (Min et al., 2021).

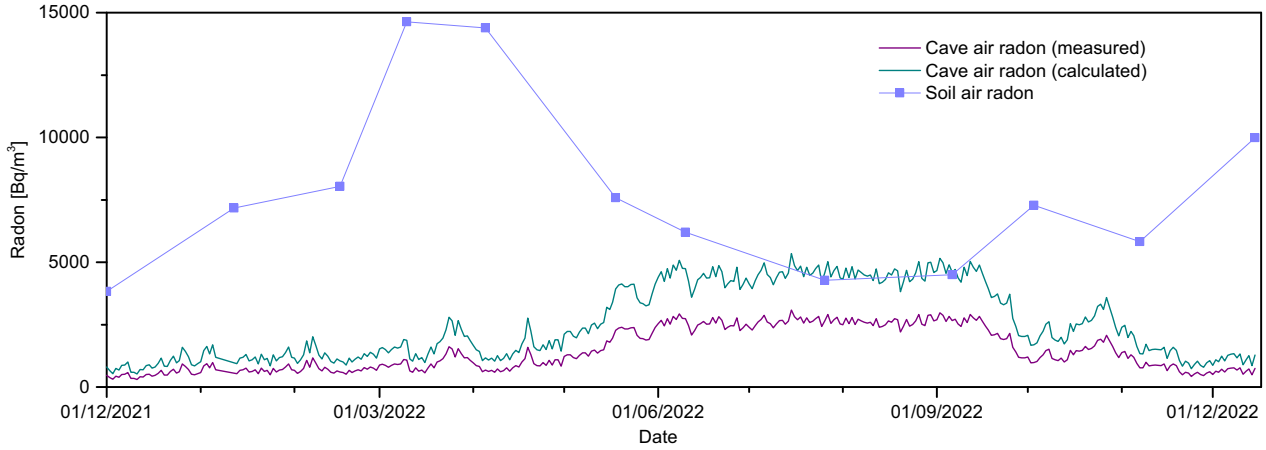

Fig. 7. Radon activity inside the Rull Cave calculated (green) by reversing 3 days of radon decay (applying Eq. (3)) to the measured (purple) radon activity in the cave air. Comparison with the soil air radon activity.

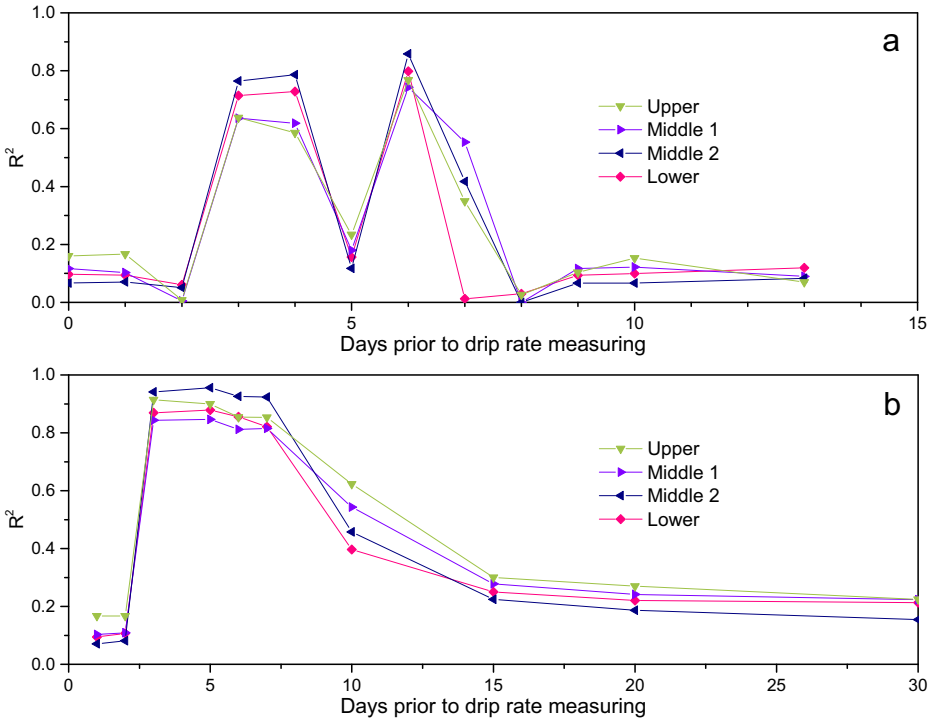

Fig. 8. (a) Coefficients of determination (R^2) between the drip rates and the absolute amount of rainfall precipitated each n day before the drip rate measuring. (b) Coefficients of determination (R^2) between the drip rates and the accumulated amount of rainfall precipitated n days before the drip rate measuring.

The evolution of CO_2 in cave waters can be naturally divided into three stages: a stage of carbonation in the soil, a stage of solution of calcite and/or dolomite, and a stage of equilibration with cave air (Holland et al., 1964). The water properties in the Rull Cave show, in general, patterns of physicochemical variations consistent with the changes that the cave air undergoes, showing a clear influence of the equilibration stage. During summer, when the cave air reaches the highest concentrations of CO_2 (Fig. 3), the increase in the partial pressure of CO_2 both in air and (calculated) in water causes a general decrease in water pH, in contrast to the higher pH measured when the cave is ventilated (Fig. 3).

The calcite saturation indices (SI) are close to the equilibrium state, but always slightly supersaturated (Fig. 3). There is a seasonal variation coincident with the annual pattern of CO_2 concentration in cave air and water pH. The saturation indices closest to zero are calculated for *Gour* 1, which also shows the most subtle seasonal trend. In summer, *Gour* 1 has the same saturation indices as the Lower drip, due to the high CO_2 concentrations inside the cave (Fig. 3). During the rest of the year, the SI at all drip sites are higher than at *Gour* 1 (Fig. 3), indicating that (1) the water undergoes higher CO_2 partial pressures such as within the soil, (2) it is able to dissolve larger amounts of calcite, increasing its SI, and (3) when it reaches the cave, the drip water maintains these higher SI. The differences among sampling sites show that calcite SI indicates the degree of chemical equilibrium between water and cave air: sites with slower drip rates (e.g., Lower site in Fig. 5) also have lower SI (Lower site in Fig. 3).

Regarding the origin of elements in solution, one of the most basic processes involving water-solid interaction in karstic environments is the dissolution of calcite, aragonite, and/or dolomite. The dissolution of carbonate minerals results in the release of Ca^{2+}, Mg^{2+}, and Sr^{2+} into the aqueous phase, providing the basis for using Ca^{2+}, Mg^{2+} and Sr^{2+} ratios (Négrel and Petelet-Giraud, 2005). Since the (element):Ca^{2+} ratios in drip water respond to the compositions of soil and host rock (Tooth and Fairchild, 2003; Zhou et al., 2011), and these are not likely to change over a year (Cheng et al., 2022), is that variations in soil and rock chemistry are considered irrelevant for this study.

Cave drip waters are expected to have a high degree of saturation (that is, a high Ca^{2+} concentration) (Rushdi et al., 2018) with respect to calcium carbonate minerals. The enhanced dissolution of different carbonate minerals and possible calcite reprecipitation produce different Mg/Ca and Sr/Ca ratios (Fairchild et al., 2000; Day and Henderson, 2013). Prior calcite precipitation (PCP), understood as the calcite precipitated from a solution due to it equilibrating with lower pCO_2 conditions before reaching the stalagmite (Fairchild et al., 2000; Treble et al., 2015), often results in a positive correlation between Sr/Ca and Mg/Ca in cave drip waters and speleothems, since the exclusion of Mg^{2+} and Sr^{2+} from this process causes an increase of these elements in residual water (Sinclair, 2011).

In the Rull Cave, the drip sites with the highest Ca^{2+} concentrations and the lowest Mg/Ca and Sr/Ca ratios are Upper, Middle 1, and Middle 2 (Fig. S2 and Fig. 9, respectively). These drip sites, located comparatively closer to the surface (Fig. 1), are expected to have these characteristics and no marked trends, likely due to shorter water residence time and therefore reduced chances of magnesian calcite reprecipitation in bedrock fractures (see, e.g., Rushdi et al., 2018). The remaining drip sites, Lower and Stored, have lower Ca^{2+} concentrations (Fig. S2) and show, in general, higher elemental ratios with more positive trends (Fig. 9), suggesting longer residence times.

According to Sinclair (2011), PCP will potentially produce a linear correlation in graphs of ln(Sr/Ca) versus ln(Mg/Ca) with a theoretical slope calculated to be ~0.88 ± 0.13 (given by published values of $(KdSr^{-1})/(KdMg^{-1})$) regardless of absolute drip water or host rock composition, which is also expected to be crossed by the linear plot. However, it is possible for incongruent calcite dissolution (ICD) to also produce a similar correlation, since Mg^{2+} and Sr^{2+} are released from calcite in this process, and thus a slope of 0.88 in such plots is a potential diagnosis of calcite–water interaction, but not enough to distinguish between PCP and ICD.

The plot ln(Sr/Ca) versus ln(Mg/Ca) (Fig. 9) reunites the data measured in all water samples. This is allowed by the model proposed by Sinclair (2011), since this property applies both to solutions in contact with limestone, and to any speleothem that precipitates from them. The

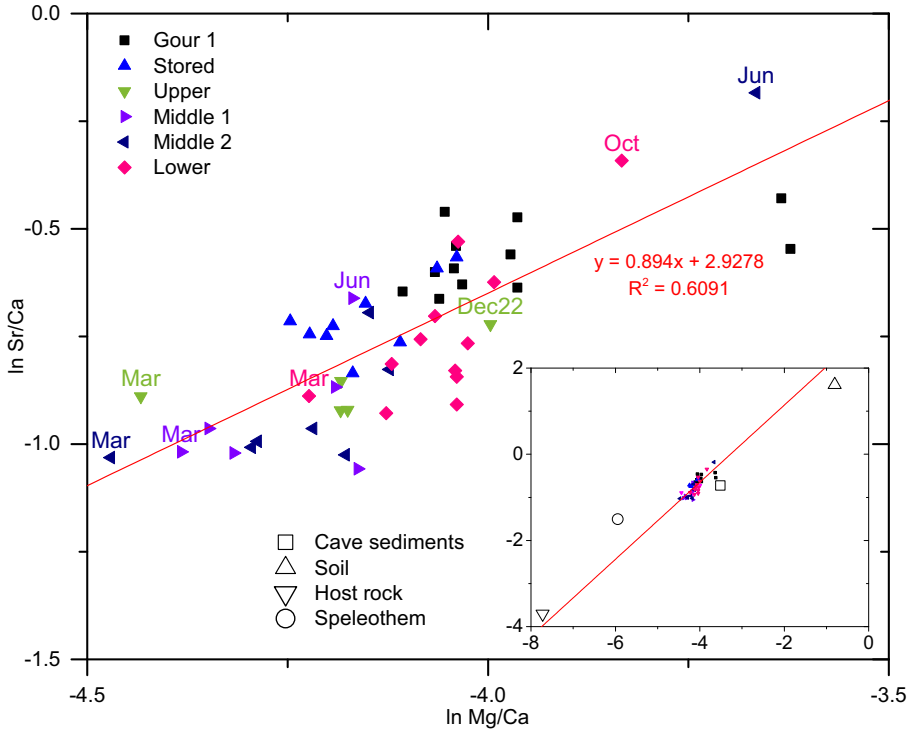

Fig. 9. ln (Mg/Ca) vs ln (Sr/Ca) plot with the corresponding trend line. The smaller graph is a zoom-out showing the location of the solid phases in the plot.

slope of the ln(Mg/Ca) vs. ln(Sr/Ca) plot for Rull Cave waters is 0.894, while the R^2 value is 0.61. This slope is close to the proposed 0.88, a significant result considering posterior studies showing that this criterion was too strict, and the PCP induced slopes could actually range from 0.709 up to 1.45 (Wassenburg et al., 2020). Fig. 9 does not show values far below the linear fitting line, which shows that, in general, water–rock interaction (WRI) does not play a major role in affecting the Mg/Ca and Sr/Ca values in the sampled water (Sinclair, 2011). This is consistent with the relatively short residence times previously estimated using radon as a tracer, and the time delay between heavy rainfall and drip rates response (Fig. 8).

Among the plotted data, the dataset which would have the slope closest to zero is that of *Gour* 1. Since the water is sampled from a cave pool, this site would have the equivalent longest residence time and a comparatively higher degree of WRI. Regarding the drip sites, the varying thickness of the vadose zone above the cave (Fig. 1) should influence the water residence time and the degree of WRI (Musgrove and Banner, 2004).

The suggested calcite–water interaction is likely to be reflected in the proportions of Mg and Sr in the formed speleothems. For instance, if PCP in the vadose zone is the main factor affecting the incorporation of Mg^{2+} and Sr^{2+} into speleothems, the higher Mg/Ca and Sr/Ca values, likely associated with lower levels of water recharge during dryer periods, will most likely be traceable in the resulting speleothems (Cruz et al., 2007).

As expected, the plotted line for the cave passes (within error) through the Mg/Ca and Sr/Ca ratios of the host rock (Fig. 9). It is also noticeable how the other solid phases of the cave system, that is, speleothem, soil, and cave sediments, are also near the fitting line.

The degree of PCP can be conditioned by the shifts in cave air CO_2. PCP is more likely to occur when the cave is ventilated, and especially at slower drip rates (Fairchild et al., 2000; Oster et al., 2012). Water flow through ventilated conduits coinciding with low cave air pCO_2 facilitates CO_2 degassing, enhancing PCP (Johnson et al., 2006) when compared to higher cave air pCO_2. Since the Rull Cave does not have a broad seasonal pCO_2 range like other caves (e.g., Treble et al., 2015; Cisneros et al., 2021), cave pCO_2 might eventually enhance or diminish PCP, but it is mainly defined by the rainfall volume and distribution throughout the year.

In particularly rainy periods, the abundant rainfalls and faster drip rates (Fig. 5) diminish or even suppress PCP, thus lowering the Sr/Ca and Mg/Ca ratios. On the contrary, the highest ratios are shown to occur during periods of scarce precipitation and slower drip rates, generally but not exclusively during summer (Fig. 5). In Fig. 9, the points corresponding to the highest and slowest drip rates are labeled with the sampling month. For each drip site, the measuring with the fastest drip rate has the lowest Mg/Ca–Sr/Ca ratios and it is, in all cases, in March 2022. This phenomenon is synchronous with the high concentrations of radon in the soil and cave air (Figs. 2 and 8), which shows the magnitude of the water infiltration. The highest Mg/Ca–Sr/Ca ratios for each drip site (Fig. 9) occur in the month with the slowest drip rates (Fig. 5).

In summary, the Lower drip site, with its low and uninterrupted flow, has more time to reach chemical equilibrium with the cave (and is more similar to *Gour* 1). The other drip sites are shown to be less in equilibrium with the cave air (as seen in the differences in pH, calcite SI, radon and chemical composition when compared to *Gour* 1) due to factors such as a thinner overlaying vadose zone, and generally faster drip rates. In this context, PCP might be considerably hindered. This is information that must be considered in studies aimed at obtaining environmental information (via trace elements) such as biogeochemical processes, bedrock dissolution and forest bioproductivity.

5.4. Cave air and drip water isotopic composition

A Keeling-plot approach (Pataki et al., 2003; Garcia-Anton et al., 2017), based on a two-end member model, confirms that the CO_2 concentration measured in cave air is the result of mixing the background atmospheric CO_2 with the soil-produced one, with the latter having a stronger influence (Fig. 10).

The points closest to the soil endmember correspond to summer, when the CO_2 concentration within the cave tends toward that of the soil. The linear fitting intercepts the y-axis at −24.5 ‰ (approaching the values of $\delta^{13}C$-CO_2 derived from C3 plant roots and microbial

respiration), as previously stated by Pla et al. (2023).

The δ^{13}C-DIC measured in *Gour* 1 has a similar annual pattern to the δ^{13}C in cave air CO_2 (Fig. 4). The δ^{13}C-DIC value in water is significantly higher due to the CO_2 degassing from the seepage water, and the water interaction with the host rock and speleothems, which cause a fractionation of carbon isotopes toward more positive values.

Fig. 6 shows the δ^{18}O and δD composition of the water sampled inside the Rull Cave, corresponding to *Gour* 1 and Stored drip. The reduced range of values indicates a smaller variability (Benettin et al., 2018), consistent with a possible buffer effect of the epikarst. The closest station with reliable rainfall isotopic data is the GNIP station in Valencia (Fig. 1), and it presents a slight but consistent shift toward higher δ^{18}O values compared to cave waters (Fig. 6). This difference can be attributed to the sampling locations: since the city of Valencia is located on the coastline, the rainfall usually derives from a vapor that originates in the sea, i.e., isotopically heavier. In the Rull Cave area, located in a valley at 470 m.a.s.l., the rainfall is possibly depleted in δ^{18}O due to the continental and altitude effects (Clark and Fritz, 1997). Therefore, the water sampled in the cave, even considering that it has probably undergone some degree of evapotranspiration, shows a lower δ^{18}O when compared to the rainfall on the coastline.

Water samples from *Gour* 1 and Stored show a seasonal distribution generally consistent with the rainfall data, with samples taken in winter having a lighter isotopic composition than those sampled during summer (Fig. 6).

In Fig. 11, the isotopic composition of the water inside the Rull Cave is compared with data from the Valencia GNIP station over a year, assuming that the isotopic composition of the rainfall at both locations has similar seasonal variations, as they are within a narrow latitude range and under the same climate type. The abovementioned difference in the isotopic composition of the rainfall between both sites is likely masked by the magnitude of the seasonal variations.

The isotopic composition of Stored drip and *Gour* 1 does not follow a noticeable seasonal pattern, but rather responds to precipitation and infiltration of rainwater into the cave. Thus, during 2022, the rainfall isotopic signal was only transmitted to the water inside the cave from December to March, which is the period when the δ^{18}O series of rainfall and the cave waters co-evolve with the same trend and similar values. Once the abundant rains in March ended, the downward trend of the δ^{18}O series of cave water reversed and no longer followed the same seasonal pattern as the δ^{18}O series of rainfall.

Some rainfall events were recorded after March, but the volume of water was not sufficient to transfer the isotopic composition to the cave. The δ^{18}O values in *Gour* 1 varied in a narrow range between −4.0 ‰ and −4.5 ‰ over the rest of the year, probably related to the slow evacuation of the water reservoir from the vadose zone above the cave. The observations are consistent with the above-described upward trend of the Sr/Ca and Mg/Ca ratios toward the summer months, which denotes a higher water–rock interaction.

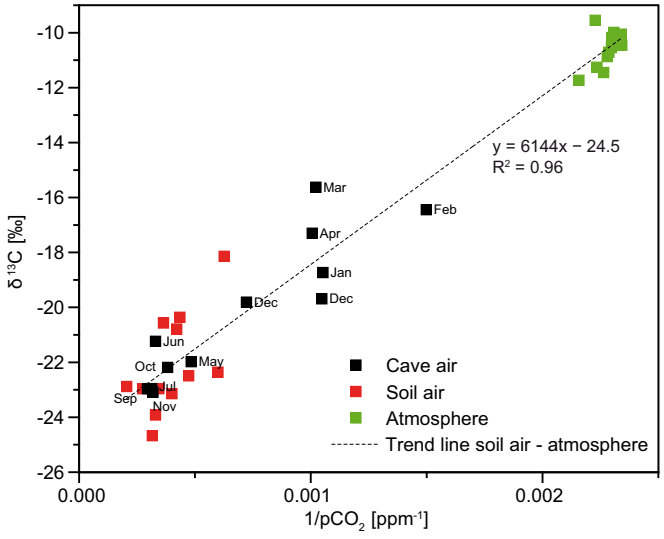

Fig. 10. Keeling plot of the air sampled inside the cave, soil, and the exterior atmosphere. Cave air samples are labeled with the month of sampling.

In summary, although the isotopic composition of rainwater becomes heavier as summer progresses, this is not transmitted to cave water due to the lack of infiltrating water: in summer 2022 there were <30 mm of rainfall in the span of approximately 100 days, while the average potential evapotranspiration for the same period was 150 mm. With the consequent decrease or discontinuation of drip sites (the few active drip sites have drip rates slower than 80 mm/h), the volume of water entering the cave is not sufficient to produce significant impacts. This causes the isotopic composition of the water inside the cave to remain relatively stable for the rest of the monitored period, and possibly stable until affected by rainfalls of sufficient magnitude to produce a shift in the water isotopic composition.

6. Conclusions

Several significant findings were drawn from the results regarding the effects of meteorological parameters, particularly rainfall, on the Rull Cave. First, the data show that the cave air gaseous concentration pattern does not only depend on the temperature-caused air mass transferences, but under the right circumstances it is also affected by events of abundant rainfall. This is best exemplified with the behavior of an inert gas such as radon, whose soil and cave activities are shown to be highly responsive to rainfall and temperature. The monitoring of radon has proven to be a useful tracer tool to study the atmosphere–soil–cave dynamics and even to estimate cave water response to rainfall. Second, the response of drip rates to rainfall events can take between 3 and 7 days, but the residence time of water might be longer, depending on the location of the dripping points relative to the soil and, thickness of the vadose zone above the cave and its configuration (fracturing degree and porosity). The drip rate response to rainfall, which is usually a longer process due to the epikarst water storage, can be reduced to a week in the case of heavy rainfall, as proven by the drip rates and the analysis of the radon series.

The main carbonate mineral, calcite, has saturation indices with a range defined by water–solid interaction, but it follows a seasonal variation pattern inversely proportional to the cave air CO_2 concentration. One of the most important processes that affect the potential use of speleothems as climate proxies is prior calcite precipitation. PCP is more likely to occur when there is a combination of slower drip rates and low pCO_2 in the underground air, although the latter is shown to be a less significant variable. The elemental ratios (Sr/Ca and Mg/Ca) show then higher sensitivity to water drip rate and rainfall response, which define the degree of water–rock interaction and the degree of water–cave air dynamic equilibrium. Outside temperatures below the cave air temperature trigger the entry of CO_2-poor air into the cave, which enhances the degassing of CO_2 from drip water and leads to higher degrees of calcite supersaturation. This is synchronous with seasonal variations in electrical conductivity, alkalinity, pH, Ca^{2+} and δ^{13}C-DIC, which is consistent with the degree of water–rock interaction. The δD and δ^{18}O composition of cave water shows a notable seasonal pattern but, individually, the δ^{18}O series indicates a strong dependence on abundant precipitations. The isotopic composition of rainfall only transfers into the epikarst during particularly rainy seasons, any seasonal pattern is hidden during the drier periods due to evapotranspiration preventing the rainfall from reaching the cave.

The Rull Cave exemplifies the complexity of karstic systems, where cave water evolves to its final composition by different pathways of gas–water–rock interaction. Therefore, cave monitoring is not only essential for assessing show caves management regarding health

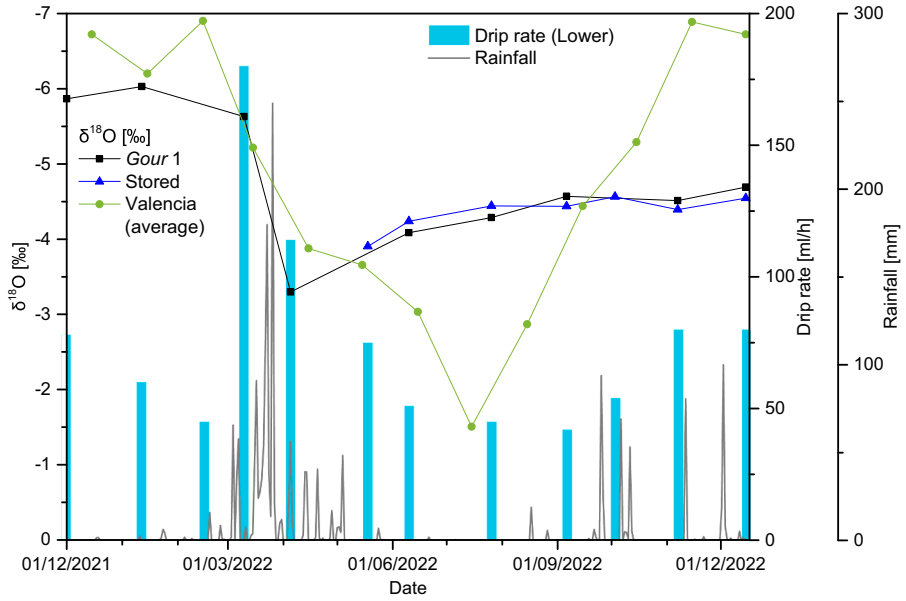

Fig. 11. $\delta^{18}O$ temporal variation compared with drip rates from Lower drip site, and the daily rainfall recorded. The plotted data of Valencia GNIP station corresponds to the monthly averages of the available series (period 2000–2021).

hazards, but also to understand the dynamics of the karstic vadose zone, which defines water quality for vast regions, responds to current climatic changes, and testifies about past climate changes by unveiling the dominant factors driving these changes. To outline, this research has advanced our understanding of Mediterranean karstic caves as the result of complex processes and interactions, by investigating the existing connection between atmospheric conditions and the cave environment. In the context of a highly changing climate, such research is an essential step regarding the preservation of karstic landscapes, and the interpretation of reliable speleothem climate records.

CRediT authorship contribution statement

M. Candela Ruiz: Writing – original draft, Visualization, Methodology, Investigation, Formal analysis, Conceptualization. **Concepción Pla:** Writing – review & editing, Supervision, Methodology, Investigation. **Angel Fernandez-Cortes:** Writing – review & editing, Resources. **David Benavente:** Writing – review & editing, Supervision, Methodology, Investigation, Funding acquisition.

Declaration of competing interest

The authors declare that they have no known competing financial interests or personal relationships that could have appeared to influence the work reported in this paper.

Data availability

Data will be made available on request.

Acknowledgements

This work was supported by the *Department of Innovation, Universities, Science and Digital Society*, *Generalitat Valenciana*, Spain [Grant number GRISOLIAP/2020/124]; *and the Ministry of Science, Innovation and Universities*, Spain [Project RTI2018-099052-BI00].

We extend our sincere gratitude to Sara Gil Oncina and Noé García Martínez (University of Alicante) for their cooperation with the sampling and monitoring conducted in the Rull Cave. We also thank Dr. Fernando Gázquez (University of Almería) for the analytical support of δD and $\delta^{18}O$ measuring in water samples.

Appendix A. Supplementary data

Supplementary data to this article can be found online at https://doi.org/10.1016/j.scitotenv.2024.171837.

References

AEMET-IM, 2011. Iberian Climate Atlas. Agencia Estatal de Meteorología (Spain) and Departamento de Meteorologia e Clima, Instituto de Meteorologia (Portugal), Madrid. https://doi.org/10.31978/784-11-002-5.

Alonso-Hernández, H., 2016. El radón en suelos, rocas, materiales de construcción y aguas subterráneas de las Islas Canarias Orientales (Doctoral thesis). Universidad de Las Palmas de Gran Canaria. http://hdl.handle.net/10553/18553.

Alvarez-Gallego, M., Garcia-Anton, E., Fernandez-Cortes, A., Cuezva, S., Sanchez-Moral, S., 2015. High radon levels in subterranean environments: monitoring and technical criteria to ensure human safety (case of Castañar Cave, Spain). J. Environ. Radioact. 145, 19–29. https://doi.org/10.1016/j.jenvrad.2015.03.024.

AVAMET - Asociación Valenciana de Meteorología 'Josep Peinado', 2023. https://www.avamet.org/mx-fitxa.php?id=c30m135e01. (Accessed 10 December 2023).

Baker, A., Berthelin, R., Cuthbert, M.O., Treble, P.C., Hartmann, A., Kss Cave Studies Team, t, 2020. Rainfall recharge thresholds in a subtropical climate determined using a regional cave drip water monitoring network. J. Hydrol. 587, 125001 https://doi.org/10.1016/j.jhydrol.2020.125001.

Baker, A., Scheller, M., Oriani, F., Mariethoz, G., Hartmann, A., Wang, Z., Cuthbert, M. O., 2021. Quantifying temporal variability and spatial heterogeneity in rainfall recharge thresholds in a montane karst environment. J. Hydrol. 594, 125965 https://doi.org/10.1016/j.jhydrol.2021.125965.

Benavente, D., Valdés-Abellán, J., Pla, C., Sanz-Rubio, E., 2019. Estimation of soil gas permeability for assessing radon risk using Rosetta pedotransfer function based on soil texture and water content. J. Environ. Radioact. 208-209 https://doi.org/10.1016/j.jenvrad.2019.105992.

Benettin, P., Volkmann, T.H.M., von Freyberg, J., Frentress, J., Penna, D., Dawson, T.E., Kirchner, J.W., 2018. Effects of climatic seasonality on the isotopic composition of evaporating soil waters. Hydrol. Earth Syst. Sci. 22, 2881–2890. https://doi.org/10.5194/hess-22-2881-2018.

Breecker, D.O., Payne, A.E., Quade, J., Banner, J.L., Ball, C.E., Meyer, K.W., Cowan, B.D., 2012. The sources and sinks of CO_2 in caves under mixed woodland and grassland vegetation. Geochim. Cosmochim. Acta 96, 230–246. https://doi.org/10.1016/j.gca.2012.08.023.

Cheng, K., Wang, Q., Liu, S., Liu, Y., Yang, Y., Zhan, C., Zhou, H., 2022. Different response of trace elements in the drip-water of Kaiyuan Cave on Shandong Peninsula (coastal North China) to hydroclimatic changes from 2012 to 2014. J. Hydrol. 608, 127616 https://doi.org/10.1016/j.jhydrol.2022.127616.

Cisneros, M., Cacho, I., Moreno, A., Stoll, H., Torner, J., Català, A., Edwards, R.L., Cheng, H., Fornós, J.J., 2021. Hydroclimate variability during the last 2700 years based on stalagmite multi-proxy records in the central-western Mediterranean. Quat. Sci. Rev. 269, 107137 https://doi.org/10.1016/j.quascirev.2021.107137.

Clark, I., Fritz, P., 1997. Environmental Isotopes in Hydrogeology. CRC Press, New York. https://doi.org/10.1201/9781482242911.
Cothern, C.R., Smith, J.E., 1987. Environmental Radon. Springer New York, New York. https://doi.org/10.1007/978-1-4899-0473-7.
Cruz, F.W., Burns, S.J., Jercinovic, M., Karmann, I., Sharp, W.D., Vuille, M., 2007. Evidence of rainfall variations in Southern Brazil from trace element ratios (Mg/Ca and Sr/Ca) in a Late Pleistocene stalagmite. Geochim. Cosmochim. Acta 71, 2250–2263. https://doi.org/10.1016/j.gca.2007.02.005.
Csondor, K., Erőss, A., Horváth, Á., Szieberth, D., 2017. Radon as a natural tracer for underwater cave exploration. J. Environ. Radioact. 173, 51–57. https://doi.org/10.1016/j.jenvrad.2016.10.020.
Day, C.C., Henderson, G.M., 2013. Controls on trace-element partitioning in cave-analogue calcite. Geochim. Cosmochim. Acta 120, 612–627. https://doi.org/10.1016/j.gca.2013.05.044.
Dreybrodt, W., 1999. Chemical kinetics, speleothem growth and climate. Boreas 28, 347–356. https://doi.org/10.1111/j.1502-3885.1999.tb00224.x.
Dumitru, O.A., Onac, B.P., Fornós, J.J., Cosma, C., Ginés, A., Ginés, J., Merino, A., 2015. Radon survey in caves from Mallorca Island, Spain. Sci. Total Environ. 526, 196–203. https://doi.org/10.1016/j.scitotenv.2015.04.076.
Fairchild, I.J., McMillan, E.A., 2007. Speleothems as indicators of wet and dry periods. Int. J. Speleol. 36, 69–74. https://doi.org/10.5038/1827-806X.36.2.2.
Fairchild, I.J., Borsato, A., Tooth, A.F., Frisia, S., Hawkesworth, C.J., Huang, Y., McDermott, F., Spiro, B., 2000. Controls on trace element (Sr–Mg) compositions of carbonate cave waters: implications for speleothem climatic records. Chem. Geol. 166, 255–269. https://doi.org/10.1016/S0009-2541(99)00216-8.
Fang, C., Moncrieff, J.B., 2001. The dependence of soil CO_2 efflux on temperature. Soil Biol. Biochem. 33, 155–165. https://doi.org/10.1016/S0038-0717(00)00125-5.
Fernandez-Cortes, A., Calaforra, J.M., Sánchez-Martos, F., 2008. Hydrogeochemical processes as environmental indicators in drip water: study of the Cueva del Agua (Southern Spain). Int. J. Speleol. 37, 41–52. https://doi.org/10.5038/1827-806X.37.1.4.
Garcia-Anton, E., Cuezva, S., Fernandez-Cortes, A., Alvarez-Gallego, M., Pla, C., Benavente, D., Cañaveras, J.C., Sanchez-Moral, S., 2017. Abiotic and seasonal control of soil-produced CO_2 efflux in karstic ecosystems located in Oceanic and Mediterranean climates. Atmos. Environ. 164, 31–49. https://doi.org/10.1016/j.atmosenv.2017.05.036.
Gavriliev, S., Petrova, T., Miklyaev, P., Karfidova, E., 2023. Predicting radon flux density from soil surface using machine learning and GIS data. Sci. Total Environ. 903, 166348 https://doi.org/10.1016/j.scitotenv.2023.166348.
Holland, H.D., Kirsipu, T.V., Huebner, J.S., Oxburgh, U.M., 1964. On some aspects of the chemical evolution of cave waters. J. Geol. 72, 36–67. https://doi.org/10.1086/626964.
Hosoda, M., Shimo, M., Sugino, M., Furukawa, M., Fukushi, M., 2007. Effect of soil moisture content on radon and thoron exhalation. J. Nucl. Sci. Technol. 44, 664–672. https://doi.org/10.1080/18811248.2007.9711855.
Huang, Y., Fairchild, I.J., Borsato, A., Frisia, S., Cassidy, N.J., McDermott, F., Hawkesworth, C.J., 2001. Seasonal variations in Sr, Mg and P in modern speleothems (Grotta di Ernesto, Italy). Chem. Geol. 175, 429–448. https://doi.org/10.1016/S0009-2541(00)00337-5.
Johnson, K.R., Hu, C., Belshaw, N.S., Henderson, G.M., 2006. Seasonal trace-element and stable-isotope variations in a Chinese speleothem: the potential for high-resolution paleomonsoon reconstruction. Earth Planet. Sci. Lett. 244, 394–407. https://doi.org/10.1016/j.epsl.2006.01.064.
Kaufman, A., Bar-Matthews, M., Ayalon, A., Carmi, I., 2003. The vadose flow above Soreq Cave, Israel: a tritium study of the cave waters. J. Hydrol. 273, 155–163. https://doi.org/10.1016/S0022-1694(02)00394-3.
Kulali, F., Akkurt, I., Özgür, N., 2017. The effect of meteorological parameters on radon concentration in soil gas. Acta Phys. Pol. A 132, 999–1001. https://doi.org/10.12693/APhysPolA.132.999.
Li, B., Yuan, D., Qin, J., Lin, Y., Zhang, M., 2000. Oxygen and carbon isotopic characteristics of rainwater, drip water and present speleothems in a cave in Guilin area, and their environmental meanings. Sci. China Ser. D Earth Sci. 43, 277–285. https://doi.org/10.1007/BF02906823.
Maeng, S., Han, S., Lee, S., 2019. Analysis of radon depth profile in soil air after a rainfall by using diffusion model. Nucl. Eng. Technol. 51, 2013–2017. https://doi.org/10.1016/j.net.2019.06.018.
McDonald, J., Drysdale, R., 2007. Hydrology of cave drip waters at varying bedrock depths from a karst system in southeastern Australia. Hydrol. Process. 21, 1737–1748. https://doi.org/10.1002/hyp.6356.
Min, K., Slessarev, E., Kan, M., McFarlane, K., Oerter, E., Pett-Ridge, J., Nuccio, E., Berhe, A.A., 2021. Active microbial biomass decreases, but microbial growth potential remains similar across soil depth profiles under deeply-vs. shallow-rooted plants. Soil Biol. Biochem. 162, 108401 https://doi.org/10.1016/j.soilbio.2021.108401.
Modibo, O.B., Tamakuma, Y., Suzuki, T., Yamada, R., Zhuo, W., Kranrod, C., Iwaoka, K., Akata, N., Hosoda, M., Tokonami, S., 2021. Long-term measurements of radon and thoron exhalation rates from the ground using the vertical distributions of their activity concentrations. Int. J. Environ. Res. Public Health 18, 1–11. https://doi.org/10.3390/ijerph18041489.
Musgrove, M., Banner, J.L., 2004. Controls on the spatial and temporal variability of vadose dripwater geochemistry: Edwards aquifer, central Texas. Geochim. Cosmochim. Acta 68, 1007–1020. https://doi.org/10.1016/j.gca.2003.08.014.
Nadal, G., Vicens, M., Perez, D., 1990. Cova del Rull (Vall d'Ebo), 017 (Ali.-017-03VE-01C-03C). https://cuevasalicante.espeleocv.org.es/. (Accessed 10 December 2023).
Nazaroff, W.W., 1992. Radon transport from soil to air. Rev. Geophys. 30, 137–160. https://doi.org/10.1029/92RG00055.
Négrel, P., Petelet-Giraud, E., 2005. Strontium isotopes as tracers of groundwater-induced floods: the Somme case study (France). J. Hydrol. 305, 99–119. https://doi.org/10.1016/j.jhydrol.2004.08.031.
Oster, J.L., Montañez, I.P., Kelley, N.P., 2012. Response of a modern cave system to large seasonal precipitation variability. Geochim. Cosmochim. Acta 91, 92–108. https://doi.org/10.1016/j.gca.2012.05.027.
Parkhurst, D.L., Appelo, C.A.J., 2013. Description of Input and Examples for PHREEQC Version 3—A Computer Program for Speciation, Batch-reaction, One-dimensional Transport, and Inverse Geochemical Calculations, vol. 6. U.S. Geological Survey, p. 497. https://pubs.usgs.gov/tm/06/a43.
Pataki, D.E., Ehleringer, J.R., Flanagan, L.B., Yakir, D., Bowling, D.R., Still, C.J., Buchmann, N., Kaplan, J.O., Berry, J.A., 2003. The application and interpretation of Keeling plots in terrestrial carbon cycle research. Glob. Biogeochem. Cycles 17. https://doi.org/10.1029/2001GB001850.
Phong Thu, H.N., Van Thang, N., Hao, L.C., 2020. The effects of some soil characteristics on radon emanation and diffusion. J. Environ. Radioact. 216, 106189 https://doi.org/10.1016/j.jenvrad.2020.106189.
Pla, C., Cuezva, S., Garcia-Anton, E., Fernandez-Cortes, A., Cañaveras, J.C., Sanchez-Moral, S., Benavente, D., 2016a. Changes in the CO_2 dynamics in near-surface cavities under a future warming scenario: factors and evidence from the field and experimental findings. Sci. Total Environ. 565, 1151–1164. https://doi.org/10.1016/j.scitotenv.2016.05.160.
Pla, C., Galiana-Merino, J.J., Cuezva, S., Fernandez-Cortes, A., Cañaveras, J.C., Benavente, D., 2016b. Assessment of CO_2 dynamics in subsurface atmospheres using the wavelet approach: from cavity–atmosphere exchange to anthropogenic impacts in Rull cave (Vall d'Ebo, Spain). Environ. Earth Sci. 75, 446. https://doi.org/10.1007/s12665-016-5325-y.
Pla, C., Cuezva, S., Martinez-Martinez, J., Fernandez-Cortes, A., Garcia-Anton, E., Fusi, N., Crosta, G.B., Cuevas-Gonzalez, J., Cañaveras, J.C., Sanchez-Moral, S., Benavente, D., 2017. Role of soil pore structure in water infiltration and CO_2 exchange between the atmosphere and underground air in the vadose zone: a combined laboratory and field approach. CATENA 149, 402–416. https://doi.org/10.1016/j.catena.2016.10.018.
Pla, C., Fernandez-Cortes, A., Cuezva, S., Galiana-Merino, J.J., Cañaveras, J.C., Sanchez-Moral, S., Benavente, D., 2020. Insights on climate-driven fluctuations of cave ^{222}Rn and CO_2 concentrations using statistical and wavelet analyses. Geofluids 2020, 8858295. https://doi.org/10.1155/2020/8858295.
Pla, C., Ruiz, M.C., Gil-Oncina, S., García-Martínez, N., Cañaveras, J.C., Cuezva, S., Fernández-Cortés, Á., Sánchez-Moral, S., Benavente, D., 2023. ^{222}Rn and CO_2 monitoring in soil and indoor atmosphere to understand changes in the gaseous dynamics of Rull cave (Spain). Environ. Earth Sci. 82, 235. https://doi.org/10.1007/s12665-023-10885-4.
Pu, J., Yuan, D., Zhao, H., Shen, L., 2014. Hydrochemical and PCO_2 variations of a cave stream in a subtropical karst area, Chongqing, SW China: piston effects, dilution effects, soil CO_2 and buffer effects. Environ. Earth Sci. 71, 4039–4049. https://doi.org/10.1007/s12665-013-2787-z.
REVIP (Spanish Network for Isotope Monitoring in Precipitation), 2023. https://www.cedex.es/centros-laboratorios/centro-estudios-tecnicas-aplicadas-ceta/lineas-actividad/red-espanola-vigilancia-isotopos-precipitacion-revip. (Accessed 10 December 2023).
Rushdi, A.I., Ersek, V., Mix, A.C., Clark, P.U., 2018. Controls on dripwater chemistry of Oregon Caves National Monument, northwestern United States. J. Hydrol. 557, 30–40. https://doi.org/10.1016/j.jhydrol.2017.12.006.
Sakoda, A., Ishimori, Y., Hanamoto, K., Kataoka, T., Kawabe, A., Yamaoka, K., 2010. Experimental and modeling studies of grain size and moisture content effects on radon emanation. Radiat. Meas. 45, 204–210. https://doi.org/10.1016/j.radmeas.2010.01.010.
Schubert, M., Schulz, H., 2002. Diurnal radon variations in the upper soil layers and at the soil-air interface related to meteorological parameters. Health Phys. 83, 91–96. https://doi.org/10.1097/00004032-200207000-00010.
Schubert, M., Buerkin, W., Peña, P., Lopez, A.E., Balcázar, M., 2006. On-site determination of the radon concentration in water samples: methodical background and results from laboratory studies and a field-scale test. Radiat. Meas. 41, 492–497. https://doi.org/10.1016/j.radmeas.2005.10.010.
Sinclair, D.J., 2011. Two mathematical models of Mg and Sr partitioning into solution during incongruent calcite dissolution: implications for dripwater and speleothem studies. Chem. Geol. 283, 119–133. https://doi.org/10.1016/j.chemgeo.2010.05.022.
Thornthwaite, C.W., 1948. An approach toward a rational classification of climate. Geogr. Rev. 38, 55–94. https://doi.org/10.2307/210739.
Tooth, A.F., Fairchild, I.J., 2003. Soil and karst aquifer hydrological controls on the geochemical evolution of speleothem-forming drip waters, Crag Cave, southwest Ireland. J. Hydrol. 273, 51–68. https://doi.org/10.1016/S0022-1694(02)00349-9.
Treble, P.C., Fairchild, I.J., Griffiths, A., Baker, A., Meredith, K.T., Wood, A., McGuire, E., 2015. Impacts of cave air ventilation and in-cave prior calcite precipitation on Golgotha Cave dripwater chemistry, southwest Australia. Quat. Sci. Rev. 127, 61–72. https://doi.org/10.1016/j.quascirev.2015.06.001.
Vieten, R., Winter, A., Warken, S.F., Schröder-Ritzrau, A., Miller, T.E., Scholz, D., 2016. Seasonal temperature variations controlling cave ventilation processes in Cueva Larga, Puerto Rico. Int. J. Speleol. 45, 7. https://doi.org/10.5038/1827-806X.45.3.1983.
Voarintsoa, N.R.G., Ratovonanahary, A.L.J., Rakotovao, A.Z.M., Bouillon, S., 2021. Understanding the linkage between regional climatology and cave geochemical parameters to calibrate speleothem proxies in Madagascar. Sci. Total Environ. 784, 147181 https://doi.org/10.1016/j.scitotenv.2021.147181.

Wassenburg, J.A., Riechelmann, S., Schröder-Ritzrau, A., Riechelmann, D.F.C., Richter, D.K., Immenhauser, A., Terente, M., Constantin, S., Hachenberg, A., Hansen, M., Scholz, D., 2020. Calcite Mg and Sr partition coefficients in cave environments: implications for interpreting prior calcite precipitation in speleothems. Geochim. Cosmochim. Acta 269, 581–596. https://doi.org/10.1016/j.gca.2019.11.011.

Zhang, H., Zhou, Z., Dong, H., Yan, L., Ding, S., Huang, J., Gong, X., Su, D., 2023. Seasonal variations of cave dripwater hydrogeochemical parameters and δ^{13}CDIC in the subtropical monsoon region and links to regional hydroclimate. Sci. Total Environ. 881, 163509 https://doi.org/10.1016/j.scitotenv.2023.163509.

Zhou, H.Y., Wang, Y., Huang, L.Y., Mai, S.Q., 2011. Speleothem Mg, Sr and Ba records during the MIS 5c-d, and implications for paleoclimate change in NE Sichuan, Central China. Chin. Sci. Bull. 56, 3445–3450. https://doi.org/10.1007/s11434-011-4681-y.